Formic Acid Oxidation at Pt/H2O Interface from Periodic DFT Calculations Integrated with a Continuum Solvation Model

ARTICLE *in* THE JOURNAL OF PHYSICAL CHEMISTRY C · OCTOBER 2009

Impact Factor: 4.77 · DOI: 10.1021/jp9059888

Formic Acid Oxidation at Pt/H_2O Interface from Periodic DFT Calculations Integrated with a Continuum Solvation Model

Hui-Fang Wang and Zhi-Pan Liu*

Shanghai Key Laboratory of Molecular Catalysis and Innovative Materials, Department of Chemistry, MOE Key Laboratory for Computational Physical Sciences, Fudan University, Shanghai 200433, China

Received: June 26, 2009; Revised Manuscript Received: August 6, 2009

As an important class of catalytic reactions, the reaction at solid/liquid interfaces is less understood at the atomic level. From a theoretical point of view, the difficulty lies at the simultaneous consideration of the extended solid surface and the dynamic liquid environment. In taking the oxidation of formic acid (HCOOH $\rightarrow$ CO_2 + H_2) at the Pt(111)/H_2O interface as the model system that has great potentials in direct fuel cells applications, this work combines density functional theory (DFT) slab calculations with a continuum solvation model to simulate the reactions at the metal/H_2O interface for the first time. The solvation effect is treated by including (i) a few explicit water molecules as the core solvation shell and (ii) an implicit continuum solvation model to take into account the long-range electrostatic interaction from water solution. We show that formic acid can be directly oxidized to CO_2 only in the presence of preadsorbed formate. Although the formate itself can not be oxidized to CO_2 at mild conditions, it helps to stabilize the formic acid adsorption configuration with the CH bond in contact with the Pt surface, which is the precursor leading to CO_2. Without the preadsorbed formate, formic acid is only able to adsorb with its carboxyl O linking to Pt, which is however difficult to decompose further. By electronic structure analyses, we show that a hydrophobic zone formed nearby the preadsorbed fomate on Pt(111) is the origin for the promoting role of formate, which demonstrates that catalytic reactions at solid/water interface can be significantly affected by modifying the affinity between surface and water.

1. Introduction

As a promising alternative to H_2 and alcohol based fuel cells, direct formic acid fuel cells (DFAFCs) have attracted great interest in the past decades.[1−8] It was generally accepted that formic acid could be oxidized to CO_2 via a dual-path mechanism,[9−14] that is, an indirect pathway via adsorbed CO (HCOOH $\rightarrow$ CO + H_2O $\rightarrow$ CO_2 + 2H) or a direct one without the participation of CO (HCOOH $\rightarrow$ CO_2 + 2H). The presence of non-CO channel is unique and significant since CO as a poisoning species to Pt electrode is not desirable in fuel cells. Despite its significance, it remains unclear how the non-CO pathway occurs at the Pt/water interface.[15−18] Here, we carried out density functional theory slab calculations in combination with a continuum solvation model to understand HCOOH degradation on Pt(111) in the presence of water. Our results demonstrate the intimate relation among the solvation effect, the adsorption configuration, and the reaction kinetics.

To enhance the non-CO pathway while suppressing CO poisoning, many different materials have been tested, such as Pt bimetallic (PtRu,[19−21] PtPd,[19,20] PtAu,[1,22] PtPb,[2,23] PtBi[24]) and Pd-based[25−28] electrodes. It was shown that addition of Pd or Au to Pt can enhance the electro-oxidation of formic acid via the non-CO mechanism without significant formation of adsorbed CO,[19,22] and addition of Ru, Pb to Pt improves the activity by hindering CO poisoning.[2,19,29] In particular, recent experiments showed that a Pt-FeTSPc (tetrasulfophthalocyanine) cocatalyst also exhibits an enhanced activity for the electro-oxidation of formic acid without CO poisoning.[30,31] Although these electrode materials differ significantly, experimental studies by means of combined electrochemical and in situ IR measurements suggest that the dual-path mechanism of formic acid degradation is generally present. It is therefore of great interests to reveal the atomic-level mechanism of the non-CO pathway.

Samjeske et al.[17,18,32] proposed a formate-involving pathway for formic acid oxidation on Pt featuring the adsorbed formate as an active intermediate to CO_2. Their conclusion is based on the observation that the oxidation current density of HCOOH (also for methanol[33]) versus potential curve is very similar to the potential dependence of the band intensity of the adsorbed intermediate formate. A similar conclusion was also drawn by Macia et al., who performed HCOOH electro-oxidation on Pt(111) electrodes at a low Bi coverage.[34] However, on the basis of a series of potentiodynamic measurements, Behm et al.[15,16,35] found that the adsorbed formate may be spectator species instead of active intermediates during HCOOH electro-oxidation. They proposed that CO_2 is directly obtained through the dehydrogenation of a so-called weakly adsorbed HCOOH (via neither formate nor CO). Apart from the puzzles on the mechanism, it is also peculiar that the formic acid degradation has a low efficiency at the electrochemical environment considering that the degradation is rather facile under ultrahigh vacuum (UHV) conditions. For example, Columbia et al.[36] observed that the adsorbed formic acid decomposes into CO_2 via the formate intermediate at low temperatures (<300 K) according to the thermal desorption spectroscopy and high-resolution electron energy loss spectroscopy.

Because of the complexity of formic acid−water interaction[37−39] and the difficulty to model the solid/liquid interface theoretically, there are few theoretical studies reported on the mechanism of

* Corresponding author. E-mail address: zpliu@fudan.edu.cn.

10.1021/jp9059888 CCC: $40.75
Published on Web 09/11/2009

formic acid decomposition in the Pt/H_2O system. For example, Hartnig et al.[40] studied the adsorption of formic acid in the presence of two water molecules on uncharged and charged Pt(111) using DFT. In practice, it is largely uncertain how many explicit water molecules would be enough for understanding properly the reactions at the interface. A common challenge in the field is therefore how to treat the water environment at the water/metal interface, which presumably should be accurate and efficient enough to capture the chemistry during catalytic conversion. While continuum solvent models have become a standard technique in modeling liquid environment, such a model has not been utilized in standard periodical slab calculations for studying reactions at the solid/liquid interface. In this work, we have implemented the recently proposed continuum solvent model via the dielectric model function[41] into standard periodical slab calculations to model the metal−liquid interface.

With the help of this technique, we studied thoroughly formic acid oxidation on Pt(111) in the presence of water within the DFT framework. We treat the reactions at the metal/water interface as such that the reaction center is first surrounded with explicit water molecules as the core solvation shell, and the whole slab system is then immerged in the continuum solvation environment. We show that a direct decomposition of HCOOH to CO_2 is only available in the presence of precovered formate, which helps to stabilize HCOOH adsorption with its CH bond in contact with the Pt surface. Our results rationalize the accelerated kinetics of formic acid oxidation on Pt electrodes at high formate coverages.

2. Theoretical Methods

Density Functional Theory Calculations. All DFT calculations were performed with the SIESTA package using numerical atomic orbital basis sets and Troullier-Martins norm-conserving pseudopotentials[42] (scalar relativistic for heavy elements). The exchange-correlation functional used was the generalized gradient approximation method, known as GGA-PBE.[43] The other details for the DFT calculations using SIESTA can be found elsewhere.[44] The Pt lattice constant utilized is 3.980 Å from DFT (expt 3.924 Å). The Pt(111) surface in this work for studying all surface reactions was modeled by a rectangular ($4 \times 2\sqrt{3}$) unit cell with four-layer slabs (16 Pt atoms per layer), where the top two layers were fully relaxed. A ($2 \times 2 \times 1$) *k*-point mesh according to the Monkhorst-Pack scheme was utilized to sample the First Brillouin Zone. The transition states (TSs) of reactions were located using our recently developed constrained-Broyden-minimization technique as addressed previously.[45] These DFT calculation setups were also utilized in our previous works,[44,45] where the convergence on the calculated barrier has been carefully benchmarked with the calculations using the plane-wave methods.

Continuum Solvation Model with a Smooth Dielectric Function. The detailed algorithm of this method has been addressed in the series paper by Fattebert and Gygi,[41,46,47] which has been implemented for the calculations of solvation energies of free molecules. The method introduces a smoothed step function for the permittivity of the dielectric medium,

$$\varepsilon(\rho(r)) = 1 + \frac{\varepsilon_\infty - 1}{2}\left[1 + \frac{1 - (\rho(r)/\rho_0)^{2\beta}}{1 + (\rho(r)/\rho_0)^{2\beta}}\right]$$

which approaches to ε_∞ (e.g., 78.36 for water at room temperature) asymptotically in the regions where electron density is low and is 1 in the regions where it is high. In this dielectric function, ρ_0 and β are the only two parameters: ρ_0 is the threshold of electron density ρ(r) to adjust the size of the cavity, whereas β determines the smoothness of the transition from 1 to ε_∞. According to Fattebert and Gygi, these two parameters can be chosen by fitting the experimental solvation energy value for the systems of interest.

In our studies, we introduce a large vacuum region (30 Å) along *Z* axis that separates two adjacent slabs. In the middle of the vacuum region, we define a potential zero plane as the boundary condition for the integration of Poisson−Boltzmann equation, which can be solved via the finite-difference method as described by Fattebert and Gygi. To reduce the systematic errors introduced by the finite-difference method, we solve the Poisson−Boltzmann equation twice in each electronic SCF loop with (i.e., potential V_{sol}) and without (i.e., potential V_{vac}) the implicit solution to obtain the excess potential ΔV ($= V_{sol} - V_{vac}$) due to solvation. ΔV is then added into the total potential for solving the Kohn−Sham equation. The self-consistency can be achieved within typically 30 SCF loops. In this work, ρ_0 and β are set to 0.00078 e/Bohr^3 and 1.3 respectively, to fit the experimental cohesion energy of water, that is, 9.9 kcal/mol.[41]

3. Results

3.1. Adsorption of Formic Acid at Pt(111)/H_2O Interface. As the starting point, we investigated the adsorption of formic acid, as elaborated in the following. Considering that there are two critical intermediates detected in HCOOH electro-oxidation on Pt electrodes, namely, the formate and the CO, we considered the HCOOH adsorption behaviors on both the clean and the formate and CO precovered Pt(111) surfaces in the presence of water.

Adsorption on Clean Pt(111)/H_2O Interface. We first explored the possible structures of HCOOH-$(H_2O)_n$ complexes adsorbed on Pt(111), where *n* is the number of explicit H_2O molecules in the core solvation shells, being from 1 to 6 (the detailed structures are shown in Supporting Information). From the optimized structures of the adsorbed HCOOH-$(H_2O)_n$, we noticed that the bond length of the hydroxyl in HCOOH increases from 1.06 to 1.52 Å with the increase of the number of surrounding water (*n* is from 1 to 6). Furthermore, when comparing the hydroxyl bond length in the presence and absence of the metal surface, we found that the OH bond length of the adsorbed HCOOH-$(H_2O)_n$ is generally longer (~0.2 Å) than its counterpart in the free HCOOH-$(H_2O)_n$. These suggest that the OH bond of formic acid is further activated by metal surfaces, although the OH is not in a direct contact with surface, and it turns out to be more acidic. It is noticed that as *n* is larger than 2, the first solvation shell of HCOOH features a ring-shaped structure, in which the waters link the hydroxyl (H donor) and the carbonyl (H acceptor) groups of HCOOH through H bondings. Such a H-bonding ring is also present for free HCOOH-$(H_2O)_{n>2}$ in vacuum.

Two different configurations of HCOOH-$(H_2O)_n$ were identified on Pt(111), namely, the O-down configuration and the CH-down configuration. The structures are shown in Figure 1a,b, respectively (only the representative structures with $(H_2O)_4$ were shown). In the O-down configuration, the O atom of carbonyl group attaches to a surface Pt atom forming a O−Pt bond (2.27 Å), while in the CH-down configuration, the H of CH bond points toward the surface with the distance between H and Pt being 2.31 Å.

To compare the relative stability of the configurations of adsorbed HCOOH, we need to calculate the adsorption energy

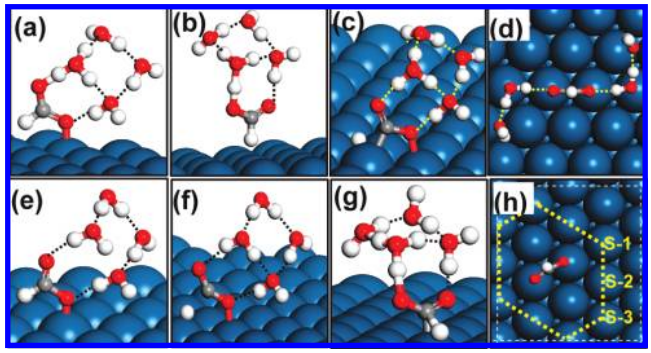

Figure 1. DFT optimized structures for key adsorbed states. (a) HCOOH-$(H_2O)_4$ adsorption in the O-down configuration; (b) HCOOH-$(H_2O)_4$ in the CH-down configuration; (c) TS for the C−H splitting of HCOOH-$(H_2O)_4$ in the O-down configuration; (d) HCOO-$(H_2O)_4$ in the bidentate configuration; (e) HCOO-$(H_2O)_4$ in the monodentate configuration; (f) TS for the C−H splitting of HCOO-$(H_2O)_4$; (g) TS for the C−H splitting of HCOOH-$(H_2O)_4$ in the CH-down configuration; (h) the neighboring sites (labeled as S-1, S-2, S-3) of an adsorbed formate on Pt(111) (also see Table 1).

of HCOOH at the metal/water interface with respect to it in the bulk water solution. This can be done as follows. From DFT, we first can obtain the adsorption energies of HCOOH-$(H_2O)_n$ complexes on Pt(111) compared to it in the vacuum, as computed from eq 1.

$$E_{ads}(\mathrm{Pt/vac}) = E^{vac}_{HCOOH-(H_2O)_n/sur} - E^{vac}_{sur} - E^{vac}_{HCOOH-(H_2O)_n} \quad (1)$$

where $E^{vac}_{HCOOH-(H_2O)_n/sur}$, E^{vac}_{sur}, and $E^{vac}_{HCOOH-(H_2O)_n}$ are the DFT total enerigies for the HCOOH complex adsorbed system, the surface without the HCOOH complex, and the free complex, respectively. Next, we can add corrections due to the solvation energy cost (ΔE_{sol}) for HCOOH-$(H_2O)_n$ complexes moving from the bulk solution to the metal/solution interface. ΔE_{sol} can be computed from eq 2, which is the solvation energy difference before and after the adsorption.

$$\Delta E_{sol} = E^{sol}_{HCOOH-(H_2O)_n/sur} - E^{sol}_{sur} - E^{sol}_{HCOOH-(H_2O)_n} \quad (2)$$

where $E^{sol}_{HCOOH-(H_2O)_n/sur}$, E^{sol}_{sur}, and $E^{sol}_{HCOOH-(H_2O)_n}$ denote the solvation energies calculated from the continuum solvation model for the adsorbed system, the surface without adsorbate, and the free HCOOH-$(H_2O)_n$, respectively. Finally, the adsorption energy of formic acid in water ($E_{ads}(Pt/H_2O)$) can be obtained as

$$E_{ads}(\mathrm{Pt/H_2O}) = E_{ads}(\mathrm{Pt/vac}) + \Delta E_{sol} \quad (3)$$

By eqs 1−3, we are able to calculate the adsorption energy of formic acid at the Pt/H_2O interface. Our calculated results are listed in Table 1, where the data for both HCOOH-$(H_2O)_4$ and HCOOH-$(H_2O)_6$ systems on clean Pt(111) are included.

Table 1 shows that the E_{ads}(Pt/vac) is converged at the level of 4 waters, where the values with 4 and 6 waters are similar ($(H_2O)_4$ as the explicit water shell was also utilized to study all of the reactions). More importantly, it can be seen that the adsorption of HCOOH in the O-down configuration at the Pt(111)/water interface (E_{ads}(Pt/H_2O)) is exothermic, while that of the CH-down configuration is thermoneutral, if not endothermic. The result suggests that formic acid adsorbs at the Pt(111)/H_2O interface with only the O-down configuration, and the CH-down configuration is unstable compared with formic acid in bulk water. This can be attributed to the intrinsic low bonding ability of the CH down configuration (E_{ads}(Pt/vac)) and an additional solvation energy cost (ΔE_{sol}) for HCOOH-$(H_2O)_n$ moving from bulk solution to the metal/solution interface. In the CH-down configuration (Figure 1b) where the hydrophilic end (hydroxyl) remains largely solvated, this ΔE_{sol} originates partly from the $-E^{sol}_{sur}$ term (eq 2), which describes the energy cost for HCOOH to exclude the interface water (or, more precisely, the dielectric layer as calculated here) on Pt(111). It is also interestingly noticed that, although the O-down configuration has an even larger ΔE_{sol}, E_{ads} at the Pt/H_2O interface remains negative, apparently because of the intrinsic strong bonding between the O of HCOOH and the Pt surface.

Adsorption on HCOO and CO Precovered Pt/H_2O Interfaces. For the HCOOH adsorption on formate precovered Pt(111), we have considered three sites near the adsorbed formate, which are labeled as S-1, S-2, and S-3 in Figure 1h. The adsorbed formate is most stable with a bidentate configuration as shown in Figure 1d (this will also be discussed in the next section). The adsorbed HCOOH was placed initially as both the O-down and the CH-down configurations. The adsorption energies are also calculated using eqs 1−3 and listed in Table 1, where the surface in eqs 1 and 2 refers to the HCOO precovered surface, and there is only implicit solvation shell for the HCOO covered surface. We found that, after the solvation energy correction, the two configurations of formic acid achieve comparable adsorption energies at the sites adjacent to the adsorbed formate. Importantly, differing from the case without the preadsorbed formate, the CH-down configuration of HCOOH turns out to be stable at the interface in the presence of formate with much improved energetics (~ -0.2 eV).

By contrast, the presence of CO affects negatively the adsorption of formic acid according to our results in Table 1. The adsorption of both configurations become energetically unfavorable ($E_{ads}(Pt/H_2O) \geq 0$) at a neighboring site (one-lattice away) of the adsorbed CO (the structure is shown in Supporting Information). This originated from the decreased E_{ads}(Pt/vac) and the increased ΔE_{sol} on the CO covered surfaces as compared with those of the clean Pt(111). Our results indicate that CO is a poisoning species for the HCOOH adsorption and oxidation.

3.2. Reaction Mechanism. Having determined the adsorption configuration of HCOOH at the Pt(111)/H_2O interface, we then studied three possible pathways for formic acid decomposition leading to CO_2. These pathways are summarized in Figure 2 with the computed reaction barriers, and the structure of the reaction intermediates labeled from a to g are shown in Figure 1. In the following, these pathways will be elaborated.

3.2.1. HCOOH Direct Degradation with the O-down Adsorption Configuration. Starting from the O-down configuration, that is, the initial state (IS), we investigated the CH bond breaking of formic acid (HCOOH-$(H_2O)_4$). The TS for the CH bond cleavage was located as shown in Figure 1c, where the dissociating CH bond is 1.61 Å. The hydroxyl of formic acid has been significantly stretched to 1.58 Å at the TS, and the forming proton is solvated by the adjacent water cluster. This is understandable as the fragment COOH is unstable in the H_2O environment and can easily lose its H (proton) to water.[48] After the TS, a CO_2 is produced directly. We found that the calculated barrier is rather high, 0.98 and 1.24 eV with and without the correction of solvation effect (hereafter the barriers at the Pt/

TABLE 1: Calculated Adsorption Energies (in eV) of Formic Acid at the Pt(111)/H_2O Interface without and with the Pre-Adsorbed Formate and CO

coverage	$(H_2O)_n$/site	O-down configuration			CH-down configuration		
		E_{ads}(Pt/vac)	ΔE_{sol}	E_{ads}(Pt/H_2O)	E_{ads}(Pt/vac)	ΔE_{sol}	E_{ads}(Pt/H_2O)
0 ML	$(H_2O)_4$	−0.55	0.40	−0.15	−0.21	0.21	0.00
	$(H_2O)_6$	−0.59	0.41	−0.18	−0.28	0.29	0.01
HCOO 0.063 ML	$(H_2O)_4$ /S-1[a]	−0.70	0.52	−0.18	−0.26	0.15	−0.11
	$(H_2O)_4$ /S-2[a]	−0.67	0.51	−0.16	−0.22	0.02	−0.20
	$(H_2O)_4$ /S-3[a]	−0.64	0.39	−0.25	−0.27	0.12	−0.15
CO 0.063 ML	$(H_2O)_4$	−0.49	0.49	0.00	−0.15	0.19	0.04

[a] Site of adsorption (S-1, S-2, S-3) nearby the formate is labeled in Figure 1h.

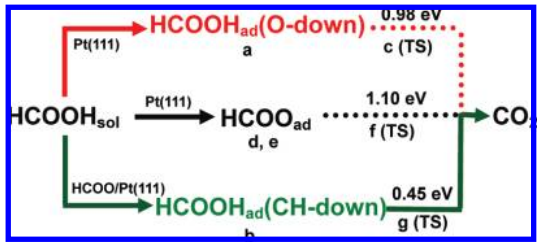

Figure 2. Three pathways for formic acid ($HCOOH_{sol}$) oxidation leading to CO_2 at Pt/H_2O interface. The data are the calculated barriers. The corresponding structures labeled from a to g are shown in Figure 1.

H_2O interface without specifically mentioning refer to the ones after the solvation energy correction). Obviously, the water solvation can better stabilize TS than IS, which reduces the barrier.[49] Since the barrier is quite high, we can rule out the possibility that formic acid itself is active in directly producing CO_2 at room temperature when Pt surface is clean.

3.2.2. HCOOH Indirect Degradation via Formate Intermediate. In this path, formic acid deprotonates first into formate. In reminding that the hydroxyl bond of formic acid at the Pt/H_2O interface has been highly activated (H−O bond length >1.5 Å), the deprotonation of formic acid is kinetically facile. Similar to the case of HCOOH-$(H_2O)_n$ adsorption, we have calculated the adsorption of HCOO-$(H_2O)_n$ complexes with up to six waters as the core solvation shells, and we found that $(H_2O)_4$ can already provide converged reaction energies for HCOOH-$(H_2O)_n$ → HCOO-$(H_2O)_n$ + 1/2H_2. From thermodynamics,[50] we can estimate the equilibrium electrical potential of the formate production by the reaction energy of HCOOH-$(H_2O)_n$ → HCOO-$(H_2O)_n$ + 1/2H_2 (see Supporting Information for detailed structures and energetics). With the zero-point energy corrections, the reaction energy is about 0.41 eV, which indicates that the equilibrium electrical potential for formate production is around 0.4 V, considering that $\Delta G = 0$ for 1/2H_2 ↔ $H^+ + e^-$ at 0 V versus NHE by definition. This coincides well with the experimental facts that the formate is detected as an important intermediate on Pt electrodes starting from low potentials (0.2−0.4 V vs NHE).[15,16,32] With the further increase of potential (above 0.4 V), it is expected that the coverage of formate will increase accordingly, as also observed in experiment.[15−18] All of the reactions were therefore performed at the $(H_2O)_4$ level, and the continuum solvation model was used to further correct the solvation energy contribution.

Since the formate is present on surface through the deprotonation of formic acid, the question is therefore whether formate can decompose to CO_2. In order to answer this, we have searched the possible pathways for formate degradation at the Pt(111)/H_2O interface. From our calculations, formate prefers a bidentate configuration (Figure 1d) at the Pt(111)/water interface, where its two O ends bond with Pt surface atoms, similar to the structure of acetate on Pt(111) as found previously.[45] This upright structure agrees with that proposed from the experimental spectroscopy.[33,51] Toward decomposition, the bidentate formate has to rotate itself first to a monodentate configuration (Figure 1e), which is the precursor leading to the H−COO bond breaking. We note that the direct C−H bond breaking from the bidentate formate is kinetically difficult with barriers more than 1.2 eV. The energy cost for the bi-to-monodentate rotation of HCOO-$(H_2O)_4$ is 0.27 eV. It may be mentioned that, in the Pt/vac system, the bi-to-monodentate rotation of HCOO is kinetically more difficult with the bidentate structure being 0.7 eV more stable than the monodentate structure. These indicate that the water environment stabilizes the monodentate configuration by a larger extent than the bidentate configuration, which smoothes the potential energy profile of the rotation.

The monodentate HCOO-$(H_2O)_4$ can then cleave its CH bond and decompose into H and CO_2 by experiencing a TS as shown in Figure 1f. At the TS, the dissociating CH bond is 1.63 Å, and the distance between C and Pt is more than 3 Å. The calculated decomposition barrier as relative to the monodentate structure is 0.83 eV, which might be relevant at high formate coverage conditions. The overall barrier is 1.10 eV with respect to the bidentate formate. By considering that the fuel cell reactions take place at room temperature, the high barrier implies that formate decomposition is very unlikely even at the high coverage conditions, which also agrees with the recent calculation results of Neurock et al.[48]

We noticed that, in the absence of H_2O (the Pt/vacuum interface), the monodentate formate follows a facile activation (barrier < 0.05 eV from our DFT) to break its CH bond, and thus formate can easily decompose at UHV conditions, as observed in experiment.[36] By contrast, in the presence of H_2O, the monodentate HCOO is strongly stabilized by solvation (H bondings) at the IS. Such a solvation effect is however largely absent at the TS where the forming CO_2 fragment is much less polarized compared with the monodentate HCOO at the IS. Therefore, at the Pt/H_2O interface, formate is much more difficult to decompose with the barrier more than 1 eV.

3.2.3. HCOOH Direct Degradation in the Presence of Preadsorbed Formate. Finally, we studied the reaction pathway of the CH bond breaking of HCOOH-$(H_2O)_4$ complex in both the CH-down and the O-down configurations in the presence of preadsorbed formate. This corresponds to an electrical potential above 0.4 V, where formate is available on the surfaces. Three sites (Figure 1h) adjacent to HCOO were considered for the reactions initially, although it was found later that the barriers for the same reaction are in fact similar at the three sites (difference within 0.05 eV). Specifically, the barrier to CH bond breaking in the O-down configuration is found to be at least 0.97 eV. This is similar to that in the absence of formate, which implies that the formate coverage influences marginally on the

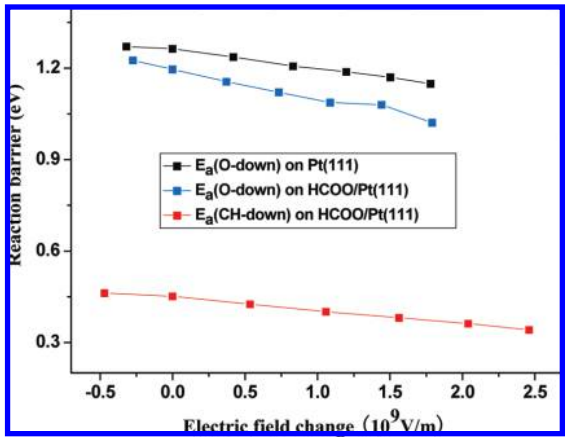

Figure 3. Barriers of the HCOOH degradation on charged Pt(111) surfaces as measured by the change of electric field. The zero in the *x* axis corresponds to the neutral surface situations.

CH-bond breaking barrier in the O-down configuration. However, we found that the CH-down configuration has a rather low barrier (0.45 eV) to break its CH bond. At the located TS (Figure 1g), the CH bond distance is 1.34 Å and the C−Pt distance is 2.26 Å. To obtain a clearer view on the reaction channel after the TS, we performed a molecular dynamics (MD) simulation at 300 K with 31 explicit H_2O molecules above Pt(111) in a $2\sqrt{3} \times 2\sqrt{3}$ Pt(111) slab (equivalent to 4 H_2O layers) by starting from the TS structure except that the dissociating CH bond is stretched further by ∼0.1 Å toward the final state. We found that after only a short period (∼0.2 ps), the hydroxylic hydrogen of the COOH fragment transfers to the surrounding water and a CO_2 is produced. It suggests that, after the CH bond breaks, the OH bond of the formic acid in the CH-down configuration can undergo a rapid activation by water leading to CO_2 formation.

3.3. Effect of Local Electric Fields on the Barrier of HCOOH Degradation. Having considered the three reaction channels for HCOOH degradation on the charge-neutral surface, we further checked whether the variation of the electric field (due to the charging of surface) can influence directly the barrier of formic acid decomposition by using our recently developed method for studying reaction under electrical potentials.[52] In the method, we can directly charge the metal surface by adding/subtracting finite electrons from the slab with the counterions being distributed as Gaussian-distributed plane charge in a vacuum. We found that the effect of the electric field induced by the excess surface charge plays only a minor role on influencing the reaction barrier, where the increase of electric field (positively charged surface as anode) will lower the barrier of all reactions considered, but the magnitude is no more than 0.07 eV per change of 10^9 V·m^{-1}, as shown in Figure 3. We can conclude that the electrochemical potential shift in a typical experiment (e.g., 0.2−0.7 V, equivalent to ∼10^9 V·m^{-1} field change) does not change significantly the reaction barrier in a direct manner. Instead, it is the potential-induced surface coverage change that strongly affects the reaction pattern of formic acid decomposition.

4. Analyses and Discussions

4.1. Physical Origin of the Solvation Effect on HCOOH Adsorption Configurations. The above results show that the formic acid can decompose into CO_2 at the Pt/H_2O interface only in the presence of preadsorbed formate. This reaction channel allows for the adsorption of formic acid with its CH bond in contact with the Pt surface. From our calculations, the adsorption configuration of formic acid is strongly influenced by the solvation energy cost (ΔE_{sol}) that measures the solvation energy change for HCOOH-$(H_2O)_n$ moving from bulk solution to the Pt/water interface. Therefore, it is essential to further explore how and why ΔE_{sol} is varied (i) with respect to the molecular orientation in adsorption and (ii) with respect to the modification of the Pt surface.

To this end, we have calculated the adsorption of small organic molecules with both hydrophobic and hydrophilic groups, namely, methanol, ethanol, and acetic acid, by utilizing the continuum solvation model (for simplicity, no explicit water was added near the organic molecules). The calculated results are listed in Table 2. We found that in general the ΔE_{sol} is lower if the molecule approaches to the metal/water interface with its alkyl group (hydrophobic end), as compared with the situation with its O-containing groups (hydrophilic end). For example, for ethanol adsorption with its OH end at the interface, its solvation energy at the interface is 0.33 eV less than ethanol in bulk water. In contrast, if ethanol is in contact with the Pt surface by its CH_3 end, ΔE_{sol} is reduced to 0.18 eV. This is reasonable as the OH end in the CH_3-down configuration remains largely exposed to water and thus to be properly solvated. Obviously, while the hydrophilic end of the molecules (e.g., the O end of HCOOH) can bond more strongly with the Pt surface, ΔE_{sol} in this configuration is also intrinsically larger because of the termination of the hydrophilic groups by surface.

In the presence of nearby adsorbed formate, the essence of the picture remains the same: the adsorption of formic acid with its O end incurs a larger ΔE_{sol} compared with that of the CH end (see Table 1). However, it is noticed that the presence of formate enlarges the difference in ΔE_{sol} between the two configurations: the ΔE_{sol} in the O-down configuration increases while that in the CH-down configuration deceases. It is this change in ΔE_{sol} that enables the adsorption of formic acid in the CH-down configuration.

To better understand the data, we have first calculated the total electrostatic potential (ESP) of the formate adsorbed Pt(111). Figure 4a,b displays the contour plots of the total ESP without and with the continuum solvation shell, respectively, showing the (111) plane cutting through the two adsorbed O of formate. It can be seen that the adsorbed formate at the Pt/water interface induces an anisotropic electrostatic potential on the plane parallel to surface: the potential is more positive at the direction perpendicular to the formate plane (*O*=C=O). The ESP pictures can be understood as follows. As formate adsorbs on the metal surface, it obtains electrons (as $HCOO^-$) from the metal Fermi surface. The accumulated electrons of formate locates mainly at its conjugated *O*=C=O π states that are perpendicular to the bonding plane. The subsequent solvation by the dielectric will lead to the further accumulation of electrons in the region, where the positive potential region is significantly enlarged in area with the continuum solvation model, as shown clearly by comparing Figure 4a,b. It can be envisioned that other molecules such as H_2O will avoid residing in this positive potential region because of the direct Pauli repulsion. As a result, the H-bonding network of water at the Pt/H_2O interface can be significantly disturbed by the presence of adsorbed formate.

To illustrate this static picture, we tentatively performed a Nose thermostat molecular dynamic simulation of adsorbed formate in the presence of H_2O molecules at 300 K (Δt = 1 fs, total simulation time 12.5 ps) within the framework of DFT-slab calculations. In MD simulation, a $2\sqrt{3} \times 2\sqrt{3}$ Pt(111) slab with 1 formate and 31 H_2O molecules (equivalent to 4 water

TABLE 2: Calculated Adsorption Energies (in eV) of Selected Organic Molecules at Pt(111)/H_2O Interface

molecules	O-down configuration			alkyl-down configuration		
	E_{ads}(Pt/vac)	ΔE_{sol}	E_{ads}(Pt/H_2O)	E_{ads}(Pt/vac)	ΔE_{sol}	E_{ads}(Pt/H_2O)
CH_3OH	−0.35	0.25	−0.10	−0.07	0.16	0.09
CH_3CH_2OH	−0.44	0.33	−0.11	0.11	0.18	0.29
CH_3COOH	−0.31	0.18	−0.13	0.05	0.04	0.09

layers) at one side of the slab was used to mimic the formate at the Pt/water interface. From the MD trajectory, we found that the first layer water molecules interact with the O end of the bidentate formate dynamically via H bonding from the direction parallel to the formate plane. Importantly, a low-water-density zone (hydrophobic) on the surface is created at the direction perpendicular to the formate plane, where water is most expelled away from the formate. In Figure 4c, we have shown a typical snapshot of the system after 10 ps (during MD, the formate is wagging on the surface, and it does not stand exactly on the top sites of two Pt atoms). We note that a 12 ps MD simulation of the Pt/H_2O interface can be not enough to obtain converged statistics; however, qualitatively the MD simulation does provide a concrete view for the above electrostatic potential analyses.

According to the above analyses, we can see that the adsorbed formate on Pt(111) can disrupt the H-bonding network of water at the metal surface by creating a long hydrophobic cavity at the direction perpendicular to the formate plane. This may explain the decrease of ΔE_{sol} in CH-down configuration and the increase of ΔE_{sol} in the O-down configuration for formic acid adsorption on the formate-covered surface (see Table 1). For the CH-down configuration, it becomes easier to exclude the interfacial water near the formate at the direction perpendicular to the formate plane. On the other hand, the adsorption with the O end cannot be solvated properly near the preadsorbed formate because of a lower water density, and thus the solvation energy cost increases.

4.2. General Implications of the Mechanism. Finally, we are at the position to address the implication of the revealed mechanism in the context of experimental findings. On the basis of our results, we suggest that the CH-down configuration of formic acid at the Pt/water interface is the only reactive precursor for CO_2 production. Furthermore, this configuration is only available at the surface sites near the adsorbed formate. From our results, we can roughly estimate that, for a formate adsorbed on Pt(111), about 10 surface sites at its neighborhood will be activated potentially for the formic acid adsorption and reaction, as outlined in Figure 1h. Therefore, the formate coverage is a key parameter for the kinetics of formic acid oxidation. This microscopic picture of reaction provides an atomic-level interpretation for the observed correlations between the current density of formic acid electro-oxidation (which is proportional to the rate of HCOOH oxidation) and the formate coverage, which showed that the increase of the Faradic current is notably faster than the increase of the coverage of formate.[15,16]

Our mechanism also sheds light on some elusive concepts in the formic acid electro-oxidation. For example, Behm et al.[15,16] suggested that the dominant reaction pathway for formic acid electro-oxidation on Pt electrodes proceeds via the "direct" oxidation of the so-called weakly adsorbed HCOOH, neither via formate nor via CO. From our results, the weakly adsorbed $HCOOH_{ad}$ species is the adsorbed formic acid in CH-down configuration, which is available when the surface is precovered with formate. The "direct" pathway corresponds to the fast dehydrogenation of the formic acid at the water/metal interface: the CH bond is activated by the Pt surface, and the H of OH is rapidly transferred to the surrounding water through the H-bonding network.

It should be interesting to mention that Zhou and co-workers[30,31] utilized modified Pt electrodes for formic acid electro-oxidation with a special promoter tetrasulfophthalocyanine (FeTSPc). They observed that nearly 1/3 Pt sites of the catalyst are covered by FeTSPc, but the modified catalyst shows much enhanced activity as compared with the nonmodified electrodes. From our analyses, the nature of the interfacial water plays important roles in the formic acid oxidation. Any added modifier, if being able to increase the surface hydrophobic properties, may enhance the catalytic activity. We expect that the promotion effect of FeTSPc may well be similar to that of formate, that is, by creating a water-exclusion zone on the surface considering the similarity between the $HCOO^-$ and the sulfonate groups of FeTSPc.

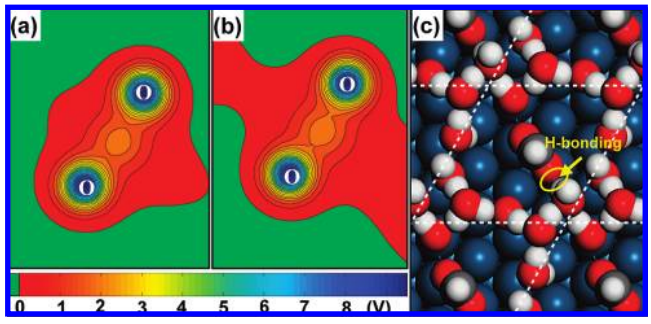

Figure 4. Formate at the Pt/H_2O interface. (a,b) Contour plots of total electrostatic potential for an adsorbed formate on Pt(111) without and with the continuum solvation shell, respectively. The planes are parallel to Pt(111) surface while cutting through the two O-ends of formate. (c) MD snapshot for a formate adsorbed in a Pt(111)/H_2O system taken after 10 ps Nose thermostat MD simulation at 300 K (only the first-layer waters are shown for clarity; see text for calculation details).

5. Conclusion

This work represents the first theoretical attempt to establish a comprehensive mechanism for formic acid oxidation at the Pt(111)/water interface. To allow for the investigation of the solid/liquid system, a continuum solvation model with a smooth dielectric function is implemented in the framework of the periodic DFT calculations, which is used to correct the solvation effect on the adsorption energetics and the reaction barriers. The method involves the solving of Poisson−Boltzmann equation by numerical finite-difference algorithm to obtain the electrostatic potential change due to the solvation, which is added to the total potential in self-consistent DFT calculations. From our results on adsorbed formic acid and formate at the Pt/H_2O interface, we found that it is essential to include both the first solvation shell of water that contains at least four explicit water molecules and the rest of the water environment as represented by the implicit continuum solvation model. Our determined mechanism of formic acid oxidation is summarized as follows.

(i) Formic acid adsorbs on Pt(111) only with the O-down configuration in the presence of H_2O environment. The O-down

configuration of formic acid is difficult to break its C−H bond with the calculated barrier around 1 eV.

(ii) Formate that is produced by the deprotonation of formic acid adsorbs on Pt with a bidentate configuration. The subsequent decomposition of formate at the Pt/H_2O interface is also difficult with the calculated barrier being 1.1 eV. By contrast, formate can decompose readily on Pt(111) in vacuum with a barrier about 0.7 eV.

(iii) In the presence of preadsorbed formate, formic acid can adsorb with the CH-down configuration near the formate. In this configuration, the CH bond of formic acid can break on Pt easily with only a 0.45 eV barrier, and a CO_2 can be formed directly since the proton of COOH can transfer to water rapidly.

We therefore conclude that formate is neither the active intermediate for CO_2 production nor the site-blocking species, but a catalyst for the direct oxidation of formic acid. By detailed analyses, we showed that the adsorbed formate disrupts the H-bonding network of water at the water/metal interfaces by creating a hydrophobic region at the direction perpendicular to the formate plane. This feature benefits the adsorption of the formic acid in the CH-down configuration by reducing the solvation energy cost of formic acid moving from the bulk solution to the metal surface. Our results rationalize the observation of the accelerated rate in HCOOH oxidation with the increase of formate coverage in electro-chemical conditions and provide valuable insights into the general pattern of catalytic reactions occurring at the metal/H_2O interface.

Acknowledgment. This work is supported by NSF of China (20825311, 20773026, 20721063, J0730419), Science & Technology Commission of Shanghai Municipality (08DZ2270500) and the Program for Professor of Special Appointment (Eastern Scholar) at Shanghai Institutions of Higher Learning.

Supporting Information Available: Optimized structures for the adsorbed HCOOH-$(H_2O)_n$ and HCOO-$(H_2O)_n$ complexes on Pt(111) (n is from 1 to 6), as well as the reaction energies for the reaction HCOOH-$(H_2O)_n$→HCOO-$(H_2O)_n$+1/2H_2. This information is available free of charge via the Internet at http://pubs.acs.org/

References and Notes

(1) Kim, J.; Jung, C.; Rhee, C. K.; Lim, T. H. *Langmuir* **2007**, *23* (21), 10831–10836.
(2) Uhm, S. Y.; Chung, S. T.; Lee, J. Y. *Electrochem. Commun.* **2007**, *9* (8), 2027–2031.
(3) Beltramo, G. L.; Shubina, T. E.; Koper, M. T. M. *ChemPhysChem* **2005**, *6* (12), 2597–2606.
(4) Wang, X.; Tang, Y.; Gao, Y.; Lu, T. H. *J. Power Sources* **2008**, *175* (2), 784–788.
(5) Miyake, H.; Okada, T.; Samjeske, G.; Osawa, M. *Phys. Chem. Chem. Phys.* **2008**, *10* (25), 3662–3669.
(6) Weber, M.; Wang, J. T.; Wasmus, S.; Savinell, R. F. *J. Electrochem. Soc.* **1996**, *143* (7), L158–L160.
(7) Yu, X. W.; Pickup, P. G. *J. Power Sources* **2008**, *182* (1), 124–132.
(8) Tian, N.; Zhou, Z. Y.; Sun, S. G.; Ding, Y.; Wang, Z. L. *Science* **2007**, *316* (5825), 732–735.
(9) Sun, S. G.; Clavilier, J.; Bewick, A. *J. Electroanal. Chem.* **1988**, *240* (1−2), 147–159.
(10) Lamy, C.; Leger, J. M. *J. Chim. Phys. Phys.-Chim. Biol.* **1991**, *88* (7−8), 1649–1671.
(11) Capon, A.; Parsons, R. *J. Electroanal. Chem.* **1973**, *45* (2), 205–231.
(12) Capon, A.; Parsons, R. *J. Electroanal. Chem.* **1973**, *44* (1), 1–7.
(13) Capon, A.; Parsons, R. *J. Electroanal. Chem.* **1975**, *65* (1), 285–305.
(14) Lovic, J. D.; Tripkovic, A. V.; Gojkovic, S. L. J.; Popovic, K. D.; Tripkovic, D. V.; Olszewski, P.; Kowal, A. *J. Electroanal. Chem.* **2005**, *581* (2), 294–302.
(15) Chen, Y. X.; Heinen, M.; Jusys, Z.; Behm, R. J. *Langmuir* **2006**, *22* (25), 10399–10408.
(16) Chen, Y. X.; Heinen, M.; Jusys, Z.; Behm, R. B. *Angew. Chem., Int. Ed.* **2006**, *45* (6), 981–985.
(17) Samjeske, G.; Osawa, M. *Angew. Chem., Int. Ed.* **2005**, *44* (35), 5694–5698.
(18) Samjeske, G.; Miki, A.; Ye, S.; Yamakata, A.; Mukouyama, Y.; Okamoto, H.; Osawa, M. *J. Phys. Chem. B* **2005**, *109* (49), 23509–23516.
(19) Rice, C.; Ha, S.; Masel, R. I.; Wieckowski, A. *J. Power Sources* **2003**, *115* (2), 229–235.
(20) Waszczuk, P.; Barnard, T. M.; Rice, C.; Masel, R. I.; Wieckowski, A. *Electrochem. Commun.* **2002**, *4* (7), 599–603.
(21) Tripkovic, A. V.; Popovic, K. D.; Lovic, J. D.; Markovic, N. M.; Radmilovic, V. *Curr. Res. Adv. Mater. Proc.* **2005**, *494*, 223–228.
(22) Choi, J. H.; Jeong, K. J.; Dong, Y.; Han, J.; Lim, T. H.; Lee, J. S.; Sung, Y. E. *J. Power Sources* **2006**, *163* (1), 71–75.
(23) Volpe, D.; Casado-Rivera, E.; Alden, L.; Lind, C.; Hagerdon, K.; Downie, C.; Korzeniewski, C.; DiSalvo, F. J.; Abruna, H. D. *J. Electrochem. Soc.* **2004**, *151* (7), A971–A977.
(24) Daniele, S.; Bergamin, S. *Electrochem. Commun.* **2007**, *9* (6), 1388–1393.
(25) Ha, S.; Larsen, R.; Masel, R. I. *J. Power Sources* **2005**, *144* (1), 28–34.
(26) Zhou, W. P.; Lewera, A.; Larsen, R.; Masel, R. I.; Bagus, P. S.; Wieckowski, A. *J. Phys. Chem. B* **2006**, *110* (27), 13393–13398.
(27) Li, X. G.; Hsing, I. M. *Electrochim. Acta* **2006**, *51* (17), 3477–3483.
(28) Brandt, K.; Steinhausen, M.; Wandelt, K. *J. Electroanal. Chem.* **2008**, *616* (1−2), 27–37.
(29) Zhang, L. J.; Wang, Z. Y.; Xia, D. G. *J. Alloys Compd.* **2006**, *426* (1−2), 268–271.
(30) Zhou, X. C.; Xing, W.; Liu, C. P.; Lu, T. H. *Electrochem. Commun.* **2007**, *9* (7), 1469–1473.
(31) Zhang, Z. G.; Zhou, X. C.; Liu, C. P.; Xing, W. *Electrochem. Commun.* **2008**, *10* (1), 131–135.
(32) Samjeske, G.; Miki, A.; Ye, S.; Osawa, M. *J. Phys. Chem. B* **2006**, *110* (33), 16559–16566.
(33) Chen, Y. X.; Miki, A.; Ye, S.; Sakai, H.; Osawa, M. *J. Am. Chem. Soc.* **2003**, *125* (13), 3680–3681.
(34) Macia, M. D.; Herrero, E.; Feliu, J. M. *J. Electroanal. Chem.* **2003**, *554*, 25–34.
(35) Chen, Y. X.; Heinen, M.; Jusys, Z.; Behm, R. J. *ChemPhysChem* **2007**, *8* (3), 380–385.
(36) Columbia, M. R.; Crabtree, A. M.; Thiel, P. A. *J. Am. Chem. Soc.* **1992**, *114* (4), 1231–1237.
(37) Columbia, M. R.; Crabtree, A. M.; Thiel, P. A. *Surf. Sci.* **1992**, *271* (1−2), 139–148.
(38) Allouche, A. *J. Chem. Phys.* **2005**, *122* (23), 234704.
(39) Wei, D. Q.; Truchon, J. F.; Sirois, S.; Salahub, D. *J. Chem. Phys.* **2002**, *116* (14), 6028–6038.
(40) Hartnig, C.; Grimminger, J.; Spohr, E. *J. Electroanal. Chem.* **2007**, *607* (1−2), 133–139.
(41) Fattebert, J. L.; Gygi, F. *J. Comput. Chem.* **2002**, *23* (6), 662–666.
(42) Soler, J. M.; Artacho, E.; Gale, J. D.; Garcia, A.; Junquera, J.; Ordejon, P.; Sanchez-Portal, D. *J. Phys.-Condes. Matter* **2002**, *14* (11), 2745–2779.
(43) Perdew, J. P.; Burke, K.; Ernzerhof, M. *Phys. Rev. Lett.* **1996**, *77* (18), 3865–3868.
(44) Wang, C. M.; Fan, K. N.; Liu, Z. P. *J. Am. Chem. Soc.* **2007**, *129* (9), 2642–2647.
(45) Wang, H. F.; Liu, Z. P. *J. Am. Chem. Soc.* **2008**, *130* (33), 10996–11004.
(46) Fattebert, J. L.; Gygi, F. *Int. J. Quantum Chem.* **2003**, *93* (2), 139–147.
(47) Fattebert, J. L.; Gygi, F. *Phys. Rev. B* **2006**, *73* (11), 115124.
(48) Neurock, M.; Janik, M.; Wieckowski, A. *Faraday Discuss.* **2008**, *140*, 363–378.
(49) Song, T.; Hu, P. J. *J. Chem. Phys.* **2006**, *125* (09), 091101.
(50) Norskov, J. K.; Rossmeisl, J.; Logadottir, A.; Lindqvist, L.; Kitchin, J. R.; Bligaard, T.; Jonsson, H. *J. Phys. Chem. B* **2004**, *108* (46), 17886–17892.
(51) Miki, A.; Ye, S.; Senzaki, T.; Osawa, M. *J. Electroanal. Chem.* **2004**, *563* (1), 23–31.
(52) Fang, Y. H.; Liu, Z. P. *J. Phys. Chem. C* **2009**, *113* (22), 9765–9772.

JP9059888